

Experimental study to evaluate the generation of reverberant shear wave fields (R-SWF) in homogenous media

Gilmer Flores
*Departamento de Ingeniería,
Pontificia Universidad Católica
del Perú,
Lima, Peru,
gilmer.flores@pucp.pe*

Juvenal Ormachea
*Department of Electrical and
Computer Engineering,
University of Rochester,
Rochester, NY, USA,
jormache@ur.rochester.edu*

Stefano E. Romero
*Departamento de Ingeniería,
Pontificia Universidad Católica
del Perú,
Lima, Peru,
sromerog@pucp.pe*

Fernando Zvietcovich
*Department of Biomedical
Engineering,
University of Houston,
Houston, TX, USA,
fzvietco@ur.rochester.edu*

Kevin J. Parker
*Department of Electrical and
Computer Engineering,
University of Rochester,
Rochester, NY, USA,
kevin.parker@rochester.edu*

Benjamin Castaneda
*Departamento de Ingeniería,
Pontificia Universidad Católica
del Perú,
Lima, Peru,
castaneda.b@pucp.edu.pe*

Abstract—In this work, we study the conditions in which a reverberant field is created by varying the number and locations of multiple mechanical sources, and then fitting axial and lateral autocorrelation profiles to theoretical models. Numerical simulation showed that at least 60 incident plane waves were necessary to generate a R-SWF. The general trend is that by applying more incident waves, the coefficient of determination improves and the error decreases. We report a bias error lower than 6% in the mean shear wave speed (C_s). Phantom experiments showed a similar tendency. Moreover, we demonstrated that the creation of a R-SWF based on the superposition of incident plane waves was possible. At least three vibration sources located at the top of the phantom surface were necessary to measure an average C_s with an error less than 9%.

Keywords—Elastography, reverberant fields, shear wave speed.

I. INTRODUCTION

Reverberant shear wave field elastography (R-SWE) is a novel imaging modality which estimates quantitative viscoelasticity parameters by applying various controlled external vibration sources in order to generate the reverberant nature of the medium creating a diffuse field within the region of interest (ROI) [1].

Ormachea et al. [2] used R-SWE in calibrated homogenous and viscoelastic phantoms, and they also analyzed the viability of the technique in breast and liver, evaluating viscoelastic parameters and the linear dispersion slope in each media. Subsequently, in [3], the results of *in vivo* multifrequency experiments on the breast, liver and kidney were reported in obese patients, confirming the penetration capacity of the reverberant field (up to 15 cm of depth). Later, Zvietcovich et al. [4] derived an improved analytic version of the physical properties of the diffuse field considering multiple transversal polarizations of shear waves.

All of the aforementioned works assume that the reverberant shear wave field exists throughout the ROI, however this is not guaranteed. Hence, the present work evaluates the generation of reverberant field of shear waves in homogeneous media for a particular geometry. A Monte Carlo analysis, considering 42 scenarios with different numbers of incident waves, was computed, using numerical simulations of the reverberant field in an elastic, isotropic, incompressible and homogeneous medium. Then, the effect of superimposing external vibration sources was validated by combining the effect of a single source placed at twelve different locations on the top surface of a gelatin-based phantom. Finally, the numerical simulations and the physical experiments were observed and compared by fitting axial and lateral autocorrelation profiles to theoretical models.

II. MATERIALS AND METHODS

A. Numerical Simulations

Numerical simulations were performed in MATLAB version R2019b (MathWorks Inc., Natick, MA, USA) using a Monte Carlo method on 42 scenarios. The mathematical model used is based on a summation of “n” incident shear waves (from 10 to 250 waves, in steps of 10, from 300 to 900 waves, in steps of 100, and, finally, from 1000 to 10,000 waves, in steps of 1000) where the uniformly distributed random input variables considered were the propagation direction vector, the displacement direction vector, which depend on the parameters in spherical coordinates, the magnitude of the particle displacement speed ([0,1] m/s) and the phase ([0, 2 π] rad). The applied vibration frequency (f_v) was 400 Hz. The reverberant field is formed within cubic medium of $5 \times 5 \times 5$ cm³ defined with a resolution of 0.1 mm. The elasticity of this medium was established by the shear wave speed (C_s) equal to 2.5 m/s. In

addition, the angular frequency ($\omega_o = 2\pi f_i$) and the wave number ($k = \omega_o/C_s$) were considered.

Curve fittings are applied to the extracted, corrected and normalized autocorrelation profiles (plane $y=0$), based on the theoretical functions, (2) and (3) reported on [4] (Fig. 1). Only the points belonging to the central region of these functions are considered, that is, $-4 \text{ mm} \leq \Delta x \leq 4 \text{ mm}$ for the axial profile and $-5 \text{ mm} \leq \Delta z \leq 5 \text{ mm}$ for the lateral one. Thus, for each direction, the wave number (k), the underlying value of the shear wave speed (C_s), the coefficients of determination (R^2) and the relative error (% error) are estimated.

Additionally, the coefficients of determination (R^2_{axial} and R^2_{lateral}) were postulated as quality parameters, since these indicate numerically how much the generated reverberant field resembles the desired diffuse field. Therefore, events whose coefficients of determination exceed certain arbitrarily defined thresholds were considered a valid field. This process was carried out iteratively on 100 events per scenario. The probability of generating the desired reverberant field was calculated, as the fraction of favorable events among total events. Preliminary results (Fig. 1 and Table I), indicated that the coefficient of determination was greater in the axial direction ($R^2_{\text{axial}} \geq R^2_{\text{lateral}}$), in most cases. Therefore, four discrimination criteria were established in Table II.

B. Homogenous Phantom Experiments

Physical experiments were performed with a gelatin-based phantom in order to validate the effect of wave superposition for reverberant field generation. This was done using an extreme combinatorial method, which consists of determining the list of possible subsets that meet a previously established condition for a set S [5].

Twelve positions are established on the upper face of the phantom at a distance (d) from the transducer, in which the maximum pressure value is achieved in the center of the ROI. The effect produced by the normal vibration source located in each of the positions is recorded (Fig. 2). In this way, the set contains each of the determined events when the vibration source is located in position F_m . The effects overlap, forming groups of n cases, where $n = 1, 2, 3 \dots 12$. The existence of a homogeneous reverberant field is analyzed in each of the $2^{n(S)} - 1$ possible subsets (4095 cases), utilizing the same criteria used in the simulations. Finally, the propagation speed of the shear waves is estimated for each valid event and the statistics of the obtained values are observed. In order to estimate the elasticity of the medium, the procedure proposed by [2] was followed.

The homogeneous $15.3 \times 12.2 \times 5.5 \text{ cm}^3$ phantom (6% gelatin concentration) was prepared following the procedure presented by [6]. Additionally, mechanical strain-stress measurements were performed as [4]. Ultrasound images were acquired with the same elements used in [2]. An external mechanical source received a sinusoidal signal from a power amplifier, coupled to a generator of at 400 Hz signals (equipment details also on [2]). The curve fit estimator was applied taking a ROI of $1 \times 1 \text{ cm}^2$ in the center of the image. The length of the window represents approximately 2 times the estimated wavelength.

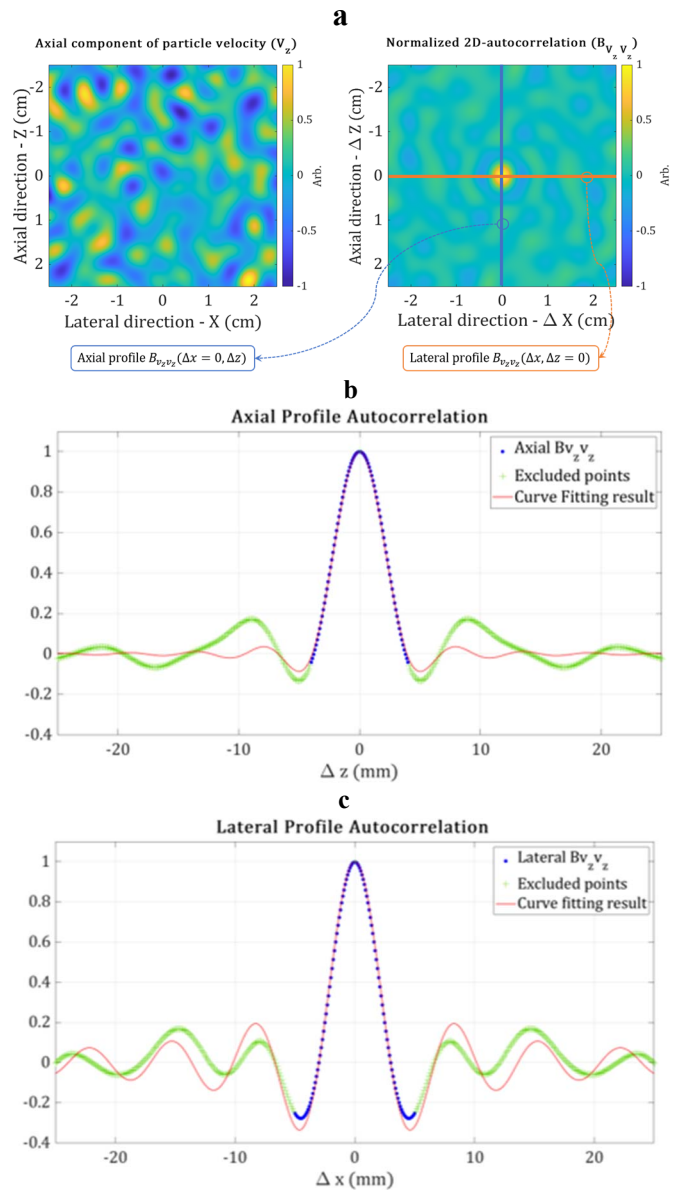


Fig. 1. Numerical simulation with 5000 incident shear waves. (a) Normalized axial component of the particle velocity and normalized 2D-autocorrelation. Extracted and fitted (b) axial and (c) lateral profiles of the autocorrelation.

TABLE I. RESULTS FROM NUMERICAL SIMULATION WITH 5000 INCIDENT SHEAR WAVES.

$C_s = 2.5 \text{ m/s}$	R^2	$k (\text{rad/m})$	$C_s (\text{m/s})$	% error
Axial	0.999	1148.02	2.19	12.43
Lateral	0.996	916.77	2.74	9.66
Mean	0.998	1032.39	2.47	1.39

TABLE II. THRESHOLDING CRITERIA.

Criteria	Numerical Simulations		Phantom Experiments
	$R^2_{\text{axial TH}}$	$R^2_{\text{lateral TH}}$	$R^2_{\text{axial TH}}$
1	0.97	0.95	0.87
2	0.92	0.90	0.82
3	0.87	0.85	0.77
4	0.82	0.80	0.72

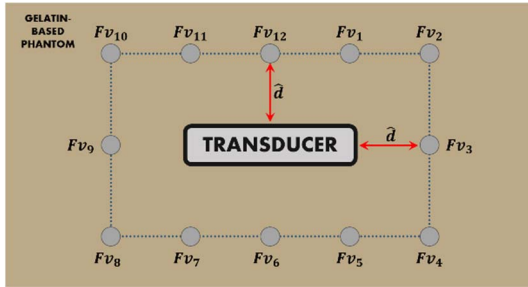


Fig. 2. Representation of the experimental setup for homogenous phantoms. 12 positions are established on the top surface of the phantom using a template.

III. RESULTS

A. Numerical Simulations

First, in Fig. 3a the results of the curve fit (CF) are displayed. The average coefficient of determination (R^2) is greater than 0.85 in all cases and increases as a function of the incident waves. R^2 reaches an estable value ($\pm 2\%$ criterion) at 60 incident waves. On the other hand, the standard deviation (σ_{R^2}) decreases, becoming less than 0.03 for 80 incident waves. Fig. 3b shows that the error of the estimate of C_s was less than 6% and reached a relative average error of less than 0.9%, in the case of 20 waves. An increase in the relative error was noted, which was established around 4.3%, from approximately 60 waves. The CF precision increased, decreasing the standard deviation to a coefficient of variation (CV) less than 8% for 80 waves and equal to 3.8% for 10,000 waves.

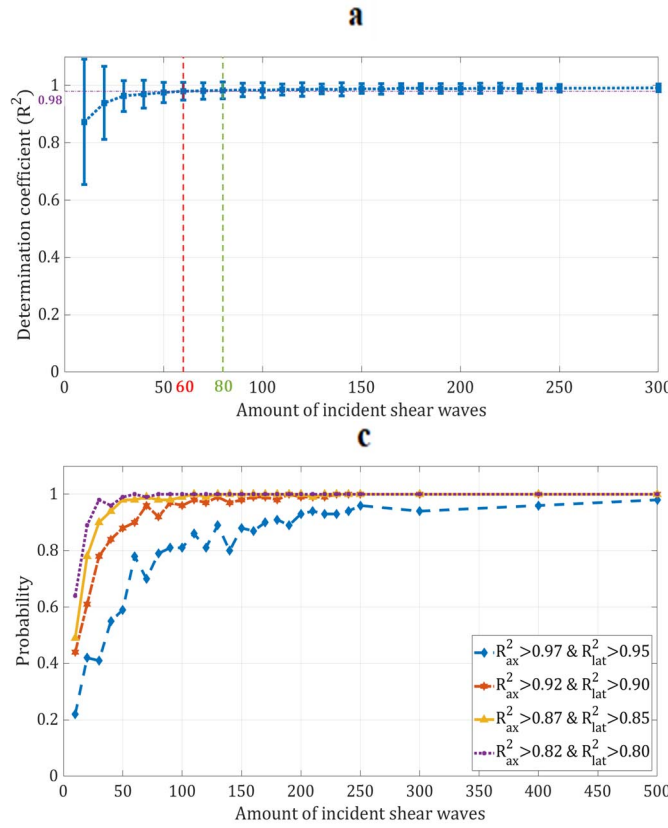


Fig. 3c shows the evolution of the probability to generate a reverberant field, applying the four criteria described on Table II. The dispersion of the percentage of relative error of estimation based on the R^2_{axial} and $R^2_{lateral}$ obtained in the cases of 10, 50 and 80 incident waves were analyzed. Fig. 3d shows that as the incidence of waves increases, the axial and lateral approach 1, while the error decreases markedly. This causes the sample density to be concentrated at the vertex ($R^2_{axial} = 1$, $R^2_{lateral} = 1$, % Error $C_s = 0$) after increasing the number of incident waves.

B. Homogenous Phantom Experiments

Experiments on the gelatin-based phantom with estimated C_s , by mechanical measurements, equal to 2.28 m/s are shown. In general, an $R^2_{average}$ of approximately 0.74 was obtained. The comparison of $R^2_{average}$, R^2_{axial} and $R^2_{lateral}$ based on the number of contact points is observed in Fig. 4a. Less variability was obtained for this parameter in the axial direction. The R^2_{axial} was found to be approximately 0.91.

The precision of the CF increased significantly, reaching relative errors of less than 9%. Also, the same parameters for the lateral direction are shown. The $R^2_{lateral}$ did not exceed 0.60, making CF a biased estimator, reaching relative errors greater than 42% (Fig. 4b). Finally, the four criteria in Table II were applied. The probability of generating a reverberant field is shown in Fig. 4c.

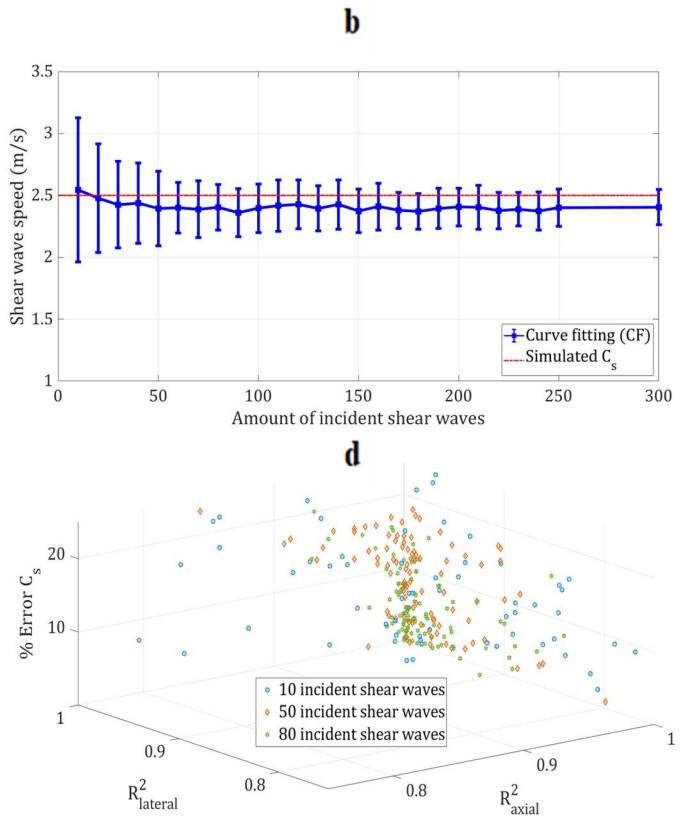


Fig. 3. (a) Mean coefficient of determination (R^2) and standard deviation (σ_{R^2}) for each scenario. (b) Estimated shear wave speed (C_s) by curve fitting. Probability to generate a R-SWF on numerical simulations. (c) Criteria from Table II were applied. (d) Dispersion of the relative error in function of the R^2_{axial} and $R^2_{lateral}$.

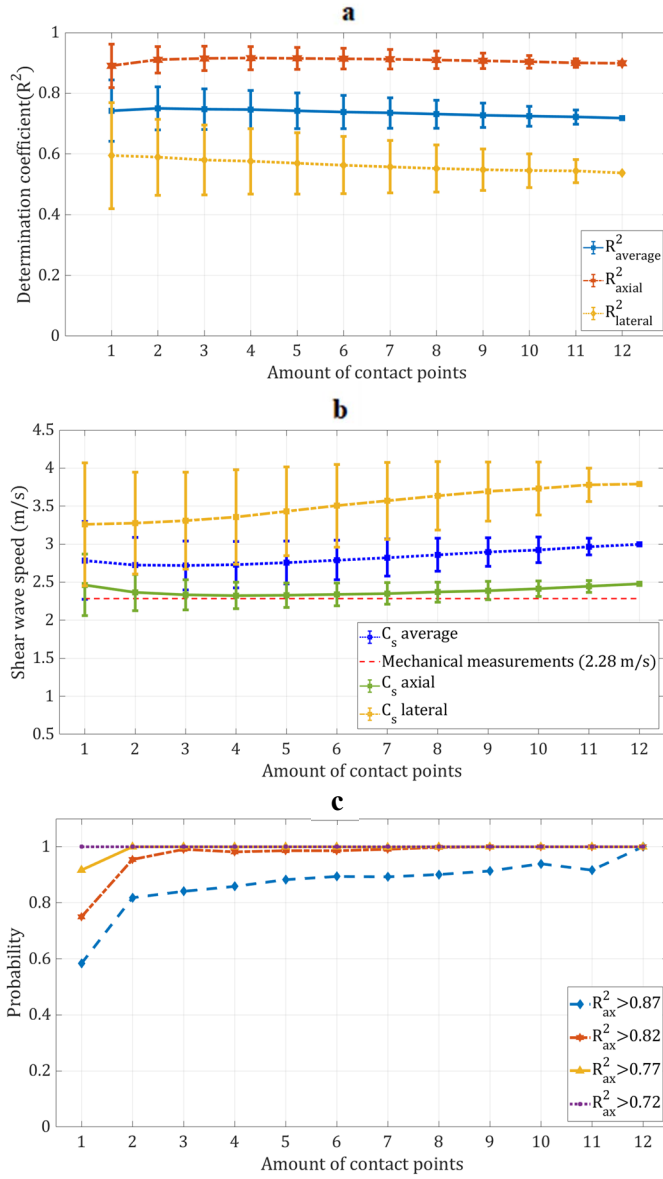


Fig. 4. (a) Coefficients of determination R^2_{average} , R^2_{axial} and R^2_{lateral} in function of the amount of contact points. (b) Axial, lateral and average shear wave speed (C_s) estimated by curve fitting. (c) Evolution of the probability to generate a R-SWF on homogenous phantom experiments. Criteria from Table II were applied.

IV. DISCUSSION AND CONCLUSIONS

The existing variation depending on the position and number of vibration sources was observed and it was shown that with a reduced number of vibration sources, it is possible to achieve relatively high values of R^2 . Precisely, between 60 and 80 incident waves in the simulations and 3 vibration sources in the physical experiments should be used to produce the desire field. The former presented R^2 greater than 0.98 with a variation of less than 0.03 and C_s with approximately 4% of bias and 7% of CV. On the other hand, the latter presented R^2_{axial} greater than 0.90 with a variation of less than 0.04 and C_s in the axial direction, with approximately 2.5% of bias and 8.5% of CV.

Although, it is essential to remember that these are deducted for a particular medium (whose attenuation value is low, allowing a greater number of reflections), the results are in agreement with previous studies reports, using 4 vibration sources in [1] and [2] or 8 rounded tips in a multi-pronged excitation ring in [4]. Furthermore, Ormachea [7] arbitrary considers that generating at least 10 incident waves in a low attenuating cubic media (6.7 Np/m at 100 Hz and characteristic length of 3 cm) could produce the desire field, which is equivalent of using more than 2 vibration sources. Thus, in this study we demonstrated that approximately more than 64% of success would be obtained, considering the same amount of incident waves, an R^2 greater than 0.8, assuming 5 Np/m of attenuation at 400 Hz, and a characteristic length of 3.3 cm (0.67 times the length of the edge [8]). Moreover, almost 100% of success in physical experiments would be reached, considering more than 2 vibration sources and a R^2_{axial} greater than 0.72.

In general, R^2 is a useful parameter to measure the quality of the R-SWF generation on a selected ROI, since it resembles the similarity degree with the theoretical models. However, its estimation is susceptible to the size of the window, the selection of excluded values and other practical settings. An example of these are the lateral direction estimators in phantom experiments, in which low values are reported, since the direct field propagated mainly axially due to the experimental setup. Further studies in non-homogeneous or anisotropic media, with reflections and diffraction effects, analyzing the estimation of elastography maps will be conducted.

ACKNOWLEDGMENT

This work was supported by Fondo Nacional de Desarrollo Científico y Tecnológico - PERU under grant 232-2018-FONDECYT from the Peruvian Government. Gilmer Flores thanks Professor Kevin Parker from the University of Rochester for all the support and help.

REFERENCES

- [1] K. J. Parker, J. Ormachea, F. Zvićcovich, and B. Castaneda, “Reverberant shear wave fields and estimation of tissue properties,” *Physics in Medicine and Biology*, vol. 62, no. 3, pp. 1046–1061, 2017.
- [2] J. Ormachea, B. Castaneda, and K. J. Parker, “Shear wave speed estimation using reverberant shear wave fields: Implementation and feasibility studies,” *Ultrasound in Medicine and Biology*, vol. 44, no. 5, pp. 963–977, 2018.
- [3] J. Ormachea, R. G. Barr, and K. J. Parker, “2-D Shear wave dispersion images using the reverberant shear wave field approach: Application in tissues exhibiting power law response,” in *IEEE International Ultrasonics Symposium, IUS*, 2019.
- [4] F. Zvićcovich, P. Pongchalee, P. Meemon, J. P. Rolland, and K. J. Parker, “Reverberant 3D optical coherence elastography maps the elasticity of individual corneal layers,” *Nature Communications*, vol. 10, no. 4895, pp. 1–13, 2019.
- [5] N. Alon and M. Krivelevich, “Extremal and probabilistic combinatorics,” in *The Princeton Companion to Mathematics*, 2010.
- [6] E. A. Gonzalez, S. E. Romero, and B. Castaneda, “Real-Time Crawling Wave Sonoelastography for Human Muscle Characterization: Initial Results,” *IEEE Transactions on Ultrasonics, Ferroelectrics, and Frequency Control*, vol. 66, no. 3, pp. 563–571, 2019.
- [7] J. Ormachea, “Viscoelastic Tissue Characterization Based on Harmonic and Transient ShearWave Elastography,” University of Rochester, Rochester, NY, USA, 2020.
- [8] A. D. Pierce, *Acoustics: An Introduction to Its Physical Principles and Applications*. 1989 Edition. 1990.